Nanotechnology Perceptions
ISSN 1660-6795
www.nano-ntp.com

Wear Analysis of 316L Stainless Steel (Implant Material) Prepared by using Powder Metallurgy Technique

R. Vishnuvardhan Reddy, B. Yeswanth Kumar Reddy, K. Pavan Kumar Reddy, S. Aparna, V. Madhusudhan Reddy

Department of mechanical Engineering, JNTUACEP, Pulivendula, Constituent colleges of Jawaharlal Nehru Technological University (JNTUA) in Anantapur, India.
E-mail: pavankumar.me@jntua.ac.in

AISI 316L stainless steel possesses favourable biocompatibility and corrosion resistance properties, rendering it exceptionally well-suited for use in medical implants, surgical equipment, and medical devices. The primary objective of this study was to investigate the wear properties of AISI 316L stainless steel (SS) that had been processed using the powder metallurgy method. The assurance of material quality was achieved through the analysis of powder particle composition, shape, and size using several techniques, including X-ray diffraction (XRD), scanning electron microscopy (SEM), and a laser scattering particle size distribution analyser. In order to generate the test specimens, a total of three cylindrical green compacts were fabricated using cold compaction. These compacts had a height of 30 mm and a diameter of 10 mm. The procedure encompassed the use of a uniaxial hydraulic press exerting a force of 10 tonnes. After the cold compaction stage, the green compacts were subjected to a sintering procedure in a controlled nitrogen atmosphere at a temperature of 1300°C for duration of 90 minutes. The implementation of a regulated environment effectively mitigated unwanted reactions that may occur during the sintering process. Following the sintering procedure, the compacts were subjected to a controlled cooling process within the furnace for duration of 12 hours until they attained ambient temperature.

The current investigation reveals that the powder material has a significant level of purity and does not manifest the existence of any supplementary elemental phases. The provided images obtained by scanning electron microscopy (SEM) illustrate granules that display a spherical form. The wear characteristics exhibit maximum performance under conditions of increased loads and accelerated sliding velocities. A higher specific wear rate was reported under a load of 20N. The experimental observations revealed that the coefficient of friction (CoF) and

the corresponding frictional force reached their minimum values when subjected to a load of 5N.
Keywords: 316L Stainless Steel, Powder Metallurgy, Wear analysis, Scanning Electron Microscopy (SEM).

1. Introduction

The utilization of steel-alloys in the field of orthopedics represents a pioneering progress in biomaterial research [1]. Even though they are less biocompatible and resistant to corrosion than titanium and similar alloys, and they wear down more quickly than cobalt-chromium alloys, stainless steel alloys, especially AISI 316L, are still used a lot in orthopedic implants. The primary factors contributing to its notable benefits are its cost-effectiveness, outstanding mechanical characteristics, elevated hardness, straightforward manufacturability, excellent resistance to corrosion, and diverse array of available product configurations. Chromium (Cr) and chromium-nickel (Cr-Ni) variants of stainless steels can be distinguished by their chemical composition [2].

Furthermore, it is worth noting that there exist five primary families, namely austenitic, ferritic, and martensitic, PH, and duplex (austenitic-ferritic), which can be generically categorized according to their microstructure [3]. The corrosion resistance of AISI 316L stainless steels is attributed to their composition, which is characterized by a low carbon content as well as high levels of nickel and chromium [4].

The initial development of metallic implants occurred during the 1960s through the utilization of powder metallurgy (P/M) techniques. The advancement of surgical implants during the past two to three decades has been facilitated by the utilization of powder metallurgy (P/M) processing techniques. P/M implants are particularly recommended in dental and orthopedic cases that necessitate a robust connection between the implant and bone, as well as a high load-bearing capacity [5,6].

The stainless steels which are manufactured through powder metallurgical route are preferred over alternative stainless steels owing to their cost-effectiveness, precise size regulation, and enhanced resistance to wear and corrosion. In recent times, there have been advancements in production procedures that have led to enhanced wear and corrosion resistance of SS (stainless steels) parts manufactured through powder metallurgy. The sintering environment has an impact on the microstructure of P/M 316L stainless steel, which is crucial to its wear mechanism [7].

Parthasarathi studied the mechanical characteristics of materials made of stainless steel (316L (N) at different room temperatures. The findings of the study indicated that increased temperatures were associated with enhanced wear rates [13]. Kurgan Naci's study looked into the effects of high sintering temperatures on AISI 316L stainless steel implant materials. The findings of the study revealed enhanced mechanical properties, an increased porosity ratio, and improved wear resistance in the implant material [14].

In his research, Manohar used powder metallurgy methods to study the AA7075/B4C/graphite biocomposite. He gradually increased the compaction pressures. The study revealed a

significant enhancement in the mechanical properties of the biocomposite [15]. Lakshmi Deepak conducted a study that investigated the influence of sintering time on the surface characteristics of wear specimens made from 316 stainless steel material. The study's conclusions showed a notable influence on the specimens' surface characteristics. [16].

The AISI 316 L stainless steel materials were fabricated using the powder metallurgy method in this study. Subsequently, the prepared specimen underwent wear testing to evaluate its features under three distinct loads: 5 N, 10 N, and 20 N.

2. Materials and methods:

2.1. Materials used:-

Gas atomized high purity AISI 316L stainless steel micropowders with particle sizes of 10µm–100µm are used for the present investigation. The chemical compositions of 316L stainless steel powders are listed in the table. 1.

Table 1: Composition of 316L Stainless Steel in weight (%)

Carbon (C)	0.029		Chromium (Cr)	17.18
Silicon (Si)	0.55		Nickel (Ni)	12.81
Manganese (Mn)	0.92		Molybdenum (Mo)	2.47
Phosphorous (P)	0.33		Nitrogen (N)	0.06
Sulphur (S)	0.007		Iron (Fe)	Balance

The scanning electron microscopy (SEM) picture of gas-atomized AISI 316L stainless steel powder particles in Figure 1(a) shows that they are shaped like spheres. To examine the purity of powder particles, the X-ray diffraction (XRD) method was used. The purity of the powders utilized is depicted in Figure 1 (b), wherein the peaks observed at 43.71, 50.79, and 74.62 (2-theta) exhibit significant intensity. This indicates the presence of more periodicity in alternative orientations. If the crystal orientation is favorable, the peak height will be elevated. The powder particles that were chosen show diffraction peaks that are consistent with the crystalline phase of 316L stainless steel, especially those related to the face-centered cubic structure (FCC). These can be seen by comparing them to the standard JCPDS card number 33-0397. The Miller indices are noted as 110, 200, 211, and 220. Also, it is noticed that there are no other elemental peaks in the XRD graph.

The Laser Scattering Particle Size Distribution Analyzer LA-960 (HORIBA) was utilized to investigate the size and distribution of the powder particles. The powder particles have a fine character, as their size ranges from 10µm to 100µm, as depicted in Figure 2. The data indicates a noticeable trend where 90% of particle sizes are reported to lie within the range of 45 to 50 µm. Figure 3 displays a variety of equipment utilized in the current study.

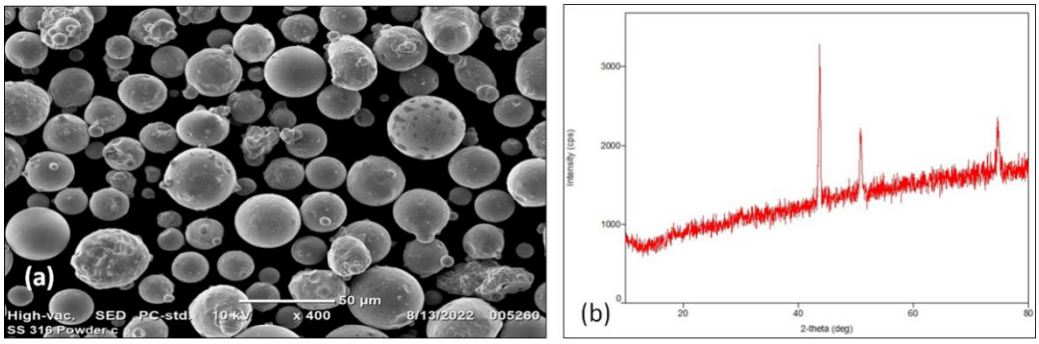

Figure 1 (a) Scanning electron microscopy (SEM) of gas-atomized AISI 316L stainless steel powder particles, (b) XRD Graph for gas-atomized AISI 316L stainless steel powder particles

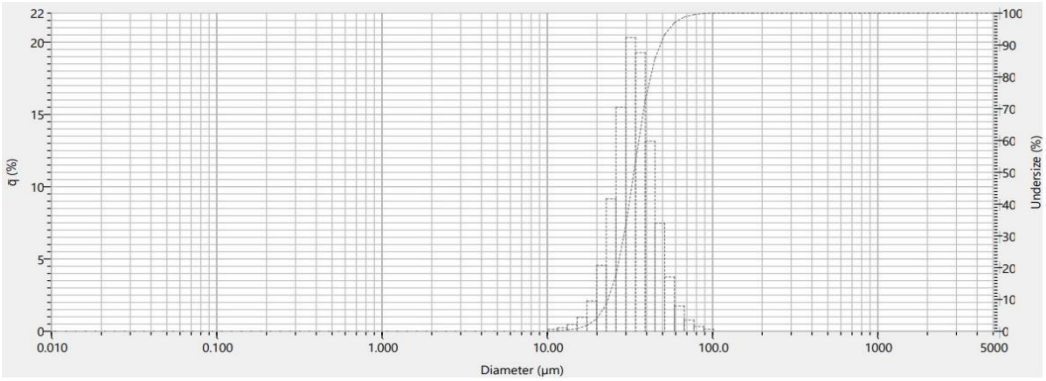

Figure 2: Powder particle distribution analysis of 316L Stainless Steel

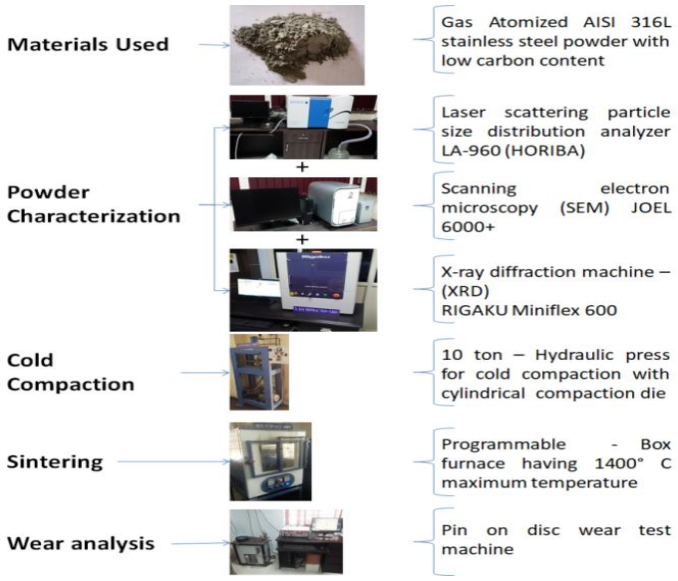

Figure 4: Variety of equipment utilized in the current study.

2.2. Specimen Preparation:-

The properties of AISI 316L stainless steel powder particles were tested in an experiment. Then, the exact amount of powder was carefully measured to get the green compact in the shape and size that was wanted. Prior to cold compaction, the 316L stainless steel powders are carefully blended with 0.6% zinc stearate, which serves as a lubricant during both mechanical milling and the subsequent cold compaction procedure. Subsequently, the entire content is homogeneously blended using a planetary mill. Table 2 enumerates the process parameters employed during the milling operation.

Table 2: Processing parameters employed during the ball milling process.

Milling Time	30 min
Used material	316L Stainless Steel
Balls make	Tungsten Carbide
Ball to powder ratio	10:1
Process control agent (PCA)	Zn-stearate
Speed of the mill	120 R.P.M

During the milling process, the particles with a spherical shape undergo a transformation and assume irregular shapes. As a consequence, the bonding between particles is significantly enhanced during the process of cold compaction. As a result, there is an enhancement in mechanical integrity, accompanied by the absence of any formation of oxide phases.

After the milling process, the resulting powder is introduced into a die made from tungsten carbide-hardened steel. Subsequently, the powder is subjected to cold compaction with a pressure of 10 tonnes (equivalent to 98066.5 N). The process is executed via an automated hydraulic press. Three specimens were produced, each with a relative density of 81% and dimensions of 30 mm in height and 10 mm in diameter, and are shown in figure 5 (a).

2.3. Sintering process: -

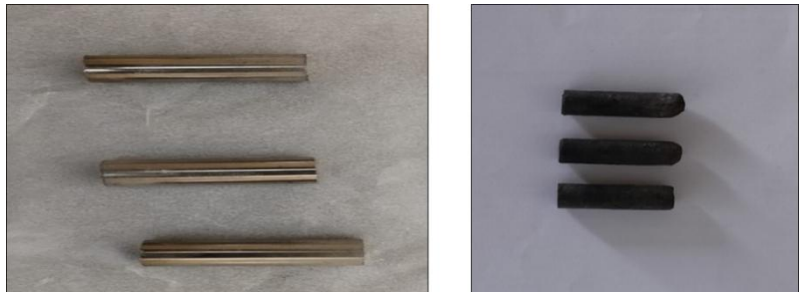

Figure 5: (a) Green compacts before sintering (b) Specimens after sintering

Following the cold compaction phase, the green compacts underwent a sintering process within a carefully regulated nitrogen environment, at a temperature of 1300°C for duration of 90 minutes. The introduction of a controlled environment successfully minimises undesired reactions that may arise during the sintering procedure. After the completion of the sintering technique, the compacts underwent a controlled cooling process within the furnace for duration of 12 hours until they reached the surrounding temperature. The elimination or

decrease in size of the pores and oxides present in the specimen is contingent upon the process of heating. A reduction in volume has been noted in the specimens in comparison to the green compacts. The sintered compacts are shown in figure 5(b).

2.4. Methodologies

Density:-

Density of the specimens after sintering is calculated by using the following Archimedes principle.

$$\text{Density} = \frac{\text{Dry weight}}{\text{Soaked weight} - \text{Suspended Weight}}$$

Wear rate calculations:-

The results from the wear tests are calculated using the below formulas.

1. % change in length of the specimens = $((W_f - W_i) / W_i) * 100$

W_i and W_f are initial and final weights of the specimens.

2. Wear Volume (V) = $((W_i - W_f) / \rho)$ in mm^3.

   $W_i - W_f$ is change in weights and ρ is density of the material.

3. Wear Velocity = $2\pi RN/60$ in mm/sec.

   R is Sliding Distance and N is Sliding Speed.

4. Wear Rate = $\frac{Wear\ Volume}{Wear\ Velocity * Load * Time}$ in mm^2/kg.

5. Wear Coefficient (X) = $\frac{Wear\ Volume * Brinell\ Hardness\ Number}{R * P}$

   P is load in kg.

6. Coefficient of friction (μ) = $\frac{F}{N}$

   F is frictional force and N is normal reaction.

3. Results and Discussion:

According to previous studies, there is a direct relationship between density and the quantity of 316L particles included in the powder formulation [9]. In order to decrease the porosity ratio of powder metallurgy (P/M) materials, it is crucial to consider significant parameters such as the size and shape of the powder grains. A reduction in the porosity ratio of powder metallurgy (P/M) materials has been found to result in enhanced mechanical properties [10]. The density of the test samples was determined utilising the Archimedes principle. The density values of the specimens have been presented in Table 4.

Table 4. Density of the specimens.

S.no	Load on the samples (N)	Density ($g/mm^{3)}$
1.	5	6.39915
2.	10	6.35
3.	20	6.52252

3.1. Wear Resistance:

The experimental setup included a pin on disc machine to perform a wear test under different normal loads. The resulting measurements included the wear volume, wear rate, percentage change in length, and wear coefficient of the specimens. There exists a clear correlation between the magnitude of the applied force and the distance over which sliding occurs, and the resulting wear volume. The load and the distance travelled have an impact on the wear rate [11]. It has been shown that an increase in loads applied to the specimens leads to a corresponding increase in both wear rate and wear volume. Nevertheless, it should be noted that the wear volume and wear rate estimates exhibit a little decrease at low sliding speeds, which might be attributed to the existence of oxide patches on the surfaces that have undergone wear [12].

During the wear testing, measurements were consistently taken to record the values of the coefficient of friction and the frictional force in relation to time. As the coefficient of friction of the specimens increases, there is an associated increase in metallic contact, which subsequently leads to increased levels of friction between the metallic surfaces. The frictional force has a positive correlation with the applied loads on the samples. The values are displayed in tables 5 and 6.

Table 5. Specific wear rate, wear volume results.

S.no	Load (Kg)	Wear Volume (mm^3)	Wear Rate (mm^2/kg)	Wear (µm)
1.	0.509858	0.0106264	$1.53568*10^{-9}$	37.06
2.	1.019716	0.003984	$2.87877*10^{-10}$	104.16
3.	2.0394	0.0026063	$9.41665*10^{-11}$	755.84

Table 6. Coefficient of friction, frictional force and wear coefficient values.

S.no	Load (kg)	Wear Coefficient (X)	Coefficient Of Friction (µ)	Frictional Force (F)	Percentage Change In Length (%)
1.	0.509858	0.037689	0.254	1.27	-0.56
2.	1.019716	0.007065	0.357	3.57	-0.20
3.	2.0394	0.002311	0.302	6.05	-0.14

3.2. Characterization of wear:

Figures 6 (a), (b), and (c) depict the observed sliding wear characteristics of 316L Stainless Steel samples subjected to loads of 5N, 10N, and 20N, respectively. The observed wear pattern demonstrates a clear and noticeable increasing trend characterised by a positive slope as the applied stresses increase [13-16]. It has been noted that the maximum wear value increased from 30µm to 760µm. The specimens saw a rise in frictional force as the loads gradually rose, resulting in an accompanying increase in material loss throughout the process of sliding wear.

Figures 7 (a) and (b) depict the comparative analysis of the frictional forces and coefficient of friction exhibited by the specimen throughout different time intervals and under varying load conditions.

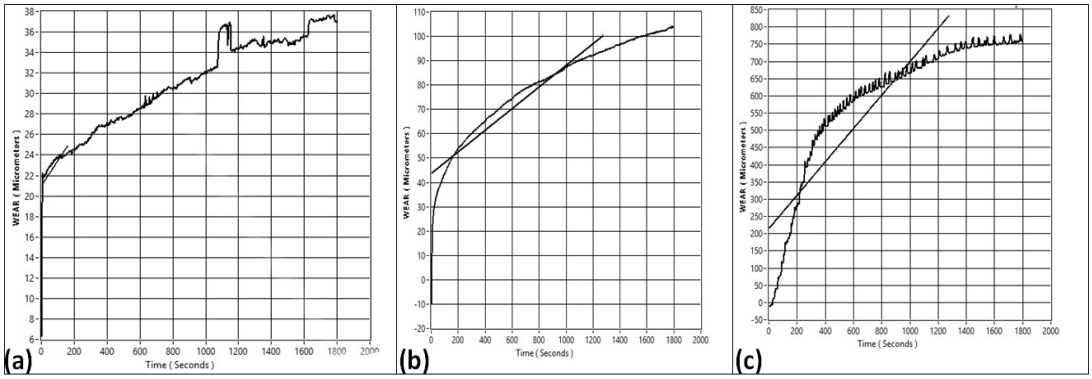

Figure 6. Wear variation over time (a) at 5 N, (b) at 10 N, and (c) at 20 N

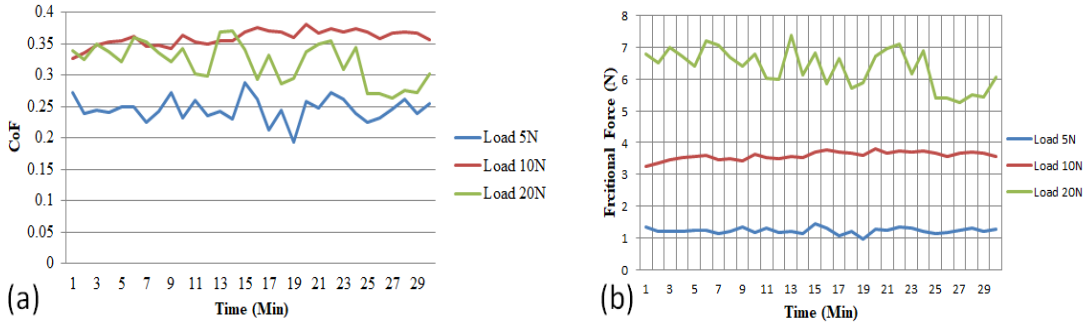

Figure 7. (a) Comparison of Coefficient of friction of specimens at loads 5, 10 & 20N, and (b) Comparison of frictional forces of specimens at loads 5, 10 & 20N

3.3. SEM Analysis:

The specimens that underwent sintering at a temperature of 1300°C exhibited worn surfaces characterised by finer grooves and wear surfaces displaying a higher number of oxygen peaks [17-20]. After the specimens underwent wear tests with varying weights, their surfaces were examined using a scanning electron microscope (SEM). The presence of scratches observed on the surfaces of the specimen provides empirical support for the occurrence of material degradation resulting from the mechanical interaction between the metallic surfaces. The scanning electron microscopy (SEM) images are depicted in Figure 8 (a-c). Additionally, the figure depicts a material surface with a low density of pores.

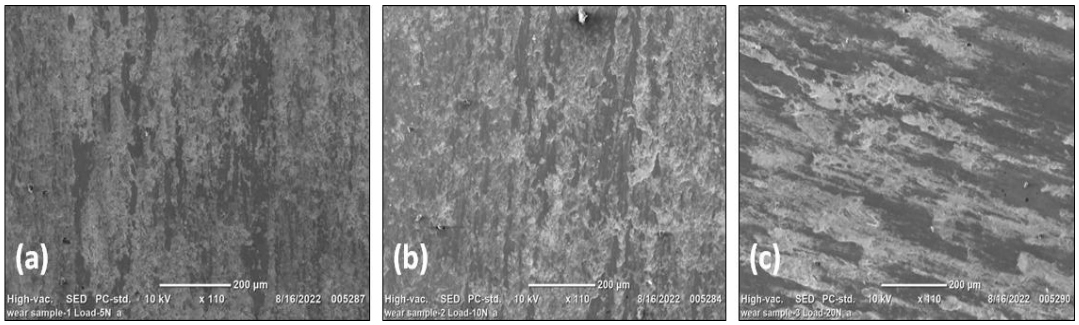

Figure 8. SEM Micrographs of wear test sample at (a) 5 N, (b) 10 N, and (c) 20 N

4. Conclusion:

The fabrication of 316L stainless steel specimens was effectively achieved by the application of powder metallurgy techniques. To summarize, the technique of X-ray diffraction was employed for the analysis of the powder particles, whereby the resulting diffraction pattern was juxtaposed with a standard reference. This comparison conclusively verified the composition of the material as 316L stainless steel, characterized by a crystal structure exhibiting face-centered cubic symmetry. The present examination indicates that the powder material exhibits a high degree of purity and does not exhibit the presence of any additional elemental phases. The scanning electron microscopy (SEM) pictures depict granules that exhibit a spherical morphology. The wear characteristics are maximized when there are elevated loads and quicker sliding speeds. When the applied stresses are increased, there is a corresponding increase in the coefficient of friction (CoF) and the resulting frictional force. A greater specific wear rate was observed when subjected to a load of 20N. The minimal values of coefficient of friction (CoF) and frictional force were observed under a load of 5N.

Acknowledgement:

Authors would like to thank Dr. VB's Ceramic Research Center for their support.

References

1. Alireza Nouri , Cuie Wen, Stainless steels in orthopedics, Structural Biomaterials, https://doi.org/10.1016/B978-0-12-818831-6.00008-2.
2. T. Newson, Stainless steel a family of medical device materials, in: Business Briefing: Medical Device Manufacturing & Technology, World Markets Research Centre, London, 2002.
3. A.S.M.T.S. Department, Technical Handbook of Stainless Steels, Atlas Specialty Metals, 2008.
4. Özbek I, Konduk B A, Bindal C, et al. Characterization of borided AISI 316L stainless steel implant. Vacuum, 2002, 65: 521–525.
5. Dabrowski J R, Oksiuta Z. Poros implantation material from vitalium alloy powder. Mater Eng, 2000, 4: 174–178.
6. Pilliar R M. P/M Processing of surgical implants: Sintered porous surfaces for tissue-to-implant fixation. Int J P/M, 1998, 34: 33–45.
7. Meng J, Loh N H, Tay B Y, et al. Tribological behavior of 316L stainless steel fabricated by micro powder injection molding. Wear, 2010, 268: 1013–1019.

8. N.L. Parthasarathi , Utpal Borah, Shaju K. Albert, Effect of temperature on sliding wear of AISI 316 L(N) stainless steel – Analysis of measured wear and surface roughness of wear tracks. Materials and Design 51 (2013) 676–682,http://dx.doi.org/10.1016/j.matdes.2013.04.050.
9. Kurgan N, Sun Y, Cicek B, et al. Production of 316L stainless steel implant materials by powder metallurgy and investigation of their wear properties. 1878, doi: 10.1007/s11434-012-5022-5 Chin Sci Bull, 2012, 57: 1873.
10. G. Manohar, K. M. Pandey and S. Ranjan Maity, Effect of compaction pressure on mechanical properties of AA7075/B4C/graphite hybrid composite fabricated by powder metallurg techniques, Materials Today:Proceedings, https://doi.org/10.1016/j.matpr.2020.05.194.
11. Lakshmi Deepak Tadepalli , Ananda Mithra Gosala , Lokesh Kondamuru , Tappa Vineeth Raj , T. Anirudh , J. Saranya , V. Vinod Kumar , Ram Subbiah, Microstructure analysis and wear characterization of AISI 316 austenitic stainless steel by cyaniding process. Materials Today: Proceedings 44 (2021) 1455–1458, https://doi.org/10.1016/j.matpr.2020.11.633.
12. Gilbert Silvaa , Márcia Regina Baldisserab , Eliandra de Sousa Trichêsc , Kátia Regina Cardoso, Preparation and Characterization of Stainless Steel 316L/HA Biocomposite. Materials Research. 2013; 16(2): 304-309, DDOI: 10.1590/S1516-14392012005000182.
13. Z. Abdullah, S. Ahmad, M. F. M. Rafter and N. S. A. Manaf, Fabrication of 316L Stainless steel foams via powder metallurgy technique. Asian Research Publishing Network (ARPN), Vol. 11, No. 12, June 2016 ISSN 1819-6608.
14. Kurgan N, Varol R. Mechanical properties of P/M 316L stainless steel materials. Powder Technol, 2010, 201: 242–247.
15. Ibrahim Orhun Tugay, A. Hosseinzadeh and Guney Guven Yapici, Hardness and wear resistance of roller burnished 316L stainless steel, Materials Today: Proceedings, https://doi.org/10.1016/j.matpr.2021.04.363.
16. R.A. García-Leon, J. Martínez-Trinidad , R. Zepeda-Bautista , I. Campos-Silva , A. Guevara-Morales , J. Martínez-Londono , J. Barbosa-Saldana, Dry sliding wear test on borided AISI 316L stainless steel under ball-on-flat configuration: A statistical analysis. Tribology International 157 (2021) 106885, https://doi.org/10.1016/j.triboint.2021.106885.
17. H. Yilmaz and R. Sadeler, Impact wear behavior of ball burnished 316L stainless steel, Surface & Coatings Technology, https://doi.org/10.1016/ j.surfcoat.2019.02.022.
18. I.G. Papantonioua, D.I. Pantelisb , D.E. Manolakosa, Powder metallurgy route aluminium zfoams: a study of the effect of powder morphology, compaction pressure and foaming temperature on the porous structure, Procedia Structural Integrity 10 (2018) 243–248, https://doi.org/10.1016/j.prostr.2018.09.034.
19. Gaurav Bajpai, Rajesh Purohit and R. S. Rana, Development of Al-Nano Composites through Powder Metallurgy Process using a newly designed Cold Isostatic Compaction Chamber, Materials Today: Proceedings 2 (2015) 2737 – 2746, https://doi.org/ 10.1016/j.matpr.2015.07.259.
20. R.A.N. Al Hakim, O. Kurdi, R. Ismail, S. Nugroho, J. Jamari, D.F. Fitriyana, M. Tauviqirrahman, A.P. Bayuseno, Mechanical Properties of AISI 316L for Artificial Hip Joint Materials Made by Investment Casting, International Journal of Advanced Research in Engineering and Technology, 11(6), 2020, pp. 175-183. https://doi.org/10.34218/IJARET.11.6.2020.016.